

# Non-equilibrium evaporation of Lennard-Jones fluids: Enskog-Vlasov theory and Hertz-Knudsen model

Shaokang Li<sup>a,b</sup>, Livio Gibelli<sup>b</sup> and Yonghao Zhang<sup>a,c</sup>

<sup>a</sup>Center for Interdisciplinary Research in Fluids, Institute of Mechanics, Chinese Academy of Sciences, Beijing, 100190, PR China

<sup>b</sup>School of Engineering, The University of Edinburgh, Edinburgh, EH9 3FQ, UK

<sup>c</sup>School of Engineering Science, University of Chinese Academy of Sciences, Beijing, 101408, PR China

## ARTICLE INFO

### Keywords:

Kinetic theory  
Enskog-Vlasov equation  
Lennard-Jones fluids  
Hertz-Knudsen model

## ABSTRACT

Enskog-Vlasov equation is currently the most sophisticated kinetic model for describing non-equilibrium evaporative flows. While it enables more efficient simulations than the molecular dynamics (MD) methods, its accuracy in reproducing the flow properties of real fluids is limited by the underlying assumptions of the Vlasov forcing term. To address this limitation, this work proposes a molecular kinetic model specifically designed for real fluids, with the Lennard-Jones fluids as an example. The model is first applied to evaluate the equilibrium characteristics of a liquid-vapour system, including the liquid-vapour coexistence curve, vapour pressure, and surface tension coefficient. The results show excellent agreement with the MD simulation and experimental data. Furthermore, the model is used to investigate non-equilibrium evaporation, with a particular focus on the velocity distribution function adjacent to the liquid-vapour interface. The findings reveal significant deviations from the Maxwellian distribution in the vapour region, suggesting that the classical Hertz-Knudsen relation becomes inaccurate when non-equilibrium effects are pronounced. Therefore, this work represents a critical step towards the development of an accurate and efficient computational framework for modelling non-equilibrium liquid-vapour flows for real fluids, with direct relevance to practical applications such as flow cooling.

## 1. Introduction


Nanoscale evaporation plays a crucial role in advancing nanotechnologies, ranging from improving substance separation efficiency in nanoporous membranes to enabling highly effective heat dissipation in high performance electronic devices (Vaartstra, Zhang, Lu, Díaz-Marín, Grossman and Wang, 2020; Dong, Poredoš, Ma and Wang, 2022; Wang, Wang, Li, Wang, Meng, Chen, Wu and Wang, 2025). However, accurate modelling of nanoscale evaporation presents a significant research challenge due to the involvement of distinct computational domains spanning multiple length and time scales.

One of the earliest and most widely-used approaches to describe the evaporation and condensation processes is the Hertz-Knudsen (HK) relation. Derived from kinetic theory, this empirical relation assumes local equilibrium in the vapour region and describes the phase change flux (evaporation or condensation) at the interface between a liquid and its vapour (Hertz, 1882; Knudsen, 1915). Its simplicity makes it particularly suited for practical applications, where detailed molecular transport effects are not the primary focus. However, at the nano/micro-scale, the HK relation overlooks the kinetic structure of the evaporation process in the Knudsen layer, a region adjacent to the liquid-vapour interface where non-equilibrium effects, such as velocity slip and temperature jump, arise due to molecular interactions. To accurately capture the complex non-equilibrium effects within the Knudsen layer, the kinetic approach is required, as

it directly accounts for molecular collisions and the kinetic structure of the evaporation process. For evaporation from a planar liquid surface, the structure of the Knudsen layer and the jump relationship along this region have been well described theoretically using the moment method to solve the Boltzmann model equations (Labuntsov and Kryukov, 1979; Meland and Yttrhus, 2003). In parallel with these theoretical investigations, numerical simulations based on the Boltzmann equation or related kinetic models have been developed to tackle this challenge across a range of flow conditions. For instance, the structure of the Knudsen layer during evaporation from a planar surface was examined using the Shakhov model (Graur, Gatapova, Wolf and Batueva, 2021). Meanwhile, the density and temperature drop in two-dimensional geometries, such as nanoporous membranes, were investigated through Direct Simulation Monte Carlo (DSMC) method (John, Enright, Sprittles, Gibelli, Emerson and Lockerby, 2019; John, Gibelli, Enright, Sprittles, Lockerby and Emerson, 2021; Li, Wang and Xia, 2021; Li, Yan and Xia, 2023). Although these approaches are well-established, they are not able to fully resolve the structure and dynamics of the liquid-vapour interface. As a result, the molecular exchange process with the liquid phase depends on a phenomenological boundary condition that requires an evaporation coefficient as an input. However, reported values for this coefficient vary by up to three orders of magnitude, introducing significant uncertainty (Persad and Ward, 2016).

To overcome the reliance on the arbitrary evaporation coefficient, a unified framework is required to cohesively describe the liquid phase, vapour phase, and their interface. The key challenge lies in accounting for the volume exclusion and molecular attraction between fluid molecules.

\*\*Corresponding author

 yonghao.zhang@imech.ac.cn (Y. Zhang)

ORCID(s):

The former has been addressed by the Enskog theory, which extends the Boltzmann equation for dense fluids, modifying the collision frequency and incorporating non-localized binary collisions. The latter is modelled by introducing a mean-field Vlasov forcing term into the Enskog equation to account for long-range forces between fluid molecules. The resulting Enskog–Vlasov (EV) equation provides a unified framework for describing non-equilibrium flows in both the liquid and vapour phases, as well as the evaporation process at the liquid–vapour interface. A notable advantage of the EV equation is that it eliminates the need for traditional evaporation models, which rely on evaporation or condensation coefficients (Enskog, 1922; Sobrino, 1967; Grmela, 1971; Karkheck and Stell, 1981). Recent studies have further demonstrated that the EV equation can describe liquid–vapour flows across a wide range of fluids and flow conditions (Frezzotti, Gibelli and Lorenzani, 2005; Barbante, Frezzotti and Gibelli, 2015; Frezzotti and Barbante, 2017; Busuioc and Gibelli, 2020).

Although the EV equation can qualitatively capture liquid–vapour flow behavior, its underlying assumptions limit its accuracy in reproducing the flow properties of real fluids. In this work, we take the Lennard-Jones fluids as an example to demonstrate how real fluids can be considered in the Enskog–Vlasov model. The Lennard-Jones potential can be expressed as (Meland and Yttrhus, 2003; Chen, Gang and Chen, 2024):

$$\phi(r) = \phi_{LJ} \left[ \left( \frac{\sigma}{r} \right)^{12} - \left( \frac{\sigma}{r} \right)^6 \right], \quad (1)$$

where the  $\phi_{LJ}$  is the potential well,  $\sigma$  is the molecular diameter, and  $r$  is the molecular distance. By contrast, in the EV equation, molecular interactions are modelled using the Sutherland potential. This assumes infinitely strong repulsion when the molecular distance is less than one diameter, reflecting the hard sphere approximation in the Enskog theory, while the attractive interactions are represented by a mean-field approximation of the attractive tail of the Lennard-Jones potential, i.e.,

$$\phi(r) = \begin{cases} +\infty, & r < \sigma, \\ -\phi_\sigma \left( \frac{\sigma}{r} \right)^6, & r \geq \sigma. \end{cases} \quad (2)$$

where  $\phi_\sigma$  is an adjusted constant parameter. It is evident that the Lennard-Jones and Sutherland potentials exhibit markedly different repulsive interaction characteristics, leading to notable difference in the fluid behaviour. For example, the critical number density  $n_c$  and critical temperature  $T_c$  of Lennard-Jones fluids are (Chung, Ajlan, Lee and Starling, 1988):

$$n_c \sigma^3 \approx 0.3185, \quad T_c = 0.3148 \frac{\phi_{LJ}}{k_B}, \quad (3)$$

where  $k_B$  is the Boltzmann constant, whereas these parameters are calculated through

$$n_c \sigma^3 \approx 0.2484, \quad T_c = 0.752 \frac{\phi_\sigma}{k_B} \quad (4)$$

in the EV framework. Although the critical temperature can be matched by adjusting  $\phi_\sigma$ , the critical reduced number density differs substantially. Therefore, it is necessary to make appropriate modifications to the EV equation to ensure consistency with the thermodynamic properties of Lennard-Jones fluids.

Although many efforts have been made to resolve this issue, there is still no kinetic model capable of accurately reproducing the two-phase flow properties of Lennard-Jones fluids with an acceptable computational cost (Benilov and Benilov, 2018, 2019; Homes, Frezzotti, Nitzke, Struchtrup and Vrabec, 2025). Based on the simplified kinetic model we have developed in our previous studies, we propose to ensure the equation of state for the Lennard-Jones fluids through modification of the pair correlation function (Wang, Wu, Ho, Li, Li and Zhang, 2020; Su, Gibelli, Li, Borg and Zhang, 2023; Shan, Su, Gibelli and Zhang, 2023; Li, Su, Shan, Li, Gibelli and Zhang, 2024; Shan, Torrilhon, Guo and Zhang, 2025), the resulting model can then reproduce critical properties of the Lennard-Jones fluids. The proposed model will first be assessed for its accuracy, including the liquid–vapour coexistence curve, vapour pressure, and surface tension coefficient. The results will also be compared with MD and experimental data to confirm whether the model can reliably predict the properties of Lennard-Jones fluids. The model will finally be employed to investigate non-equilibrium evaporation, providing detailed insights into the velocity distribution function at the interface and in the Knudsen layer. We will reveal that the molecular distribution function deviates from the Maxwellian adjacent to the interface, indicating that the HK relation becomes inaccurate under pronounced non-equilibrium conditions.

The remainder of the letter is organised as follows. Section 2 presents the simplified kinetic model and the modifications introduced to ensure the equation of state. Section 3 describes the simulations conducted under both equilibrium and non-equilibrium conditions. Finally, Section 4 summarizes the main findings and discusses future research directions.

## 2. Molecular kinetic Model

We consider a fluid composed of identical atoms interacting via the Sutherland potential (Eq. 2). The statistical behavior of this fluid is described by the molecular velocity distribution function  $f(\mathbf{x}, \boldsymbol{\xi}, t)$ , which represents the number of atoms at time  $t$  within an infinitesimal volume of single-particle phase space centered at position  $\mathbf{x}$  and molecular velocity  $\boldsymbol{\xi}$ . Following the Enskog theory for dense gases, a closed-form evolution equation for the distribution function can be derived, commonly known as the EV equation:

$$\frac{\partial f}{\partial t} + \boldsymbol{\xi} \cdot \frac{\partial f}{\partial \mathbf{x}} + \frac{\mathbf{F}}{m} \cdot \frac{\partial f}{\partial \boldsymbol{\xi}} = \Omega, \quad (5)$$

where  $\mathbf{F}$  is the self-consistent force field generated by the Sutherland potential:

$$\mathbf{F}(\mathbf{x}, t) = \int_{||\mathbf{x}_1 - \mathbf{x}|| > \sigma} \frac{d\phi}{dr} \frac{\mathbf{x}_1 - \mathbf{x}}{||\mathbf{x}_1 - \mathbf{x}||} n(\mathbf{x}_1, t) d\mathbf{x}_1, \quad (6)$$

and  $\Omega$  denotes the hard-sphere collision term derived from the Enskog theory.

While the EV equation can accurately capture the behavior of dense gases, its high computational cost limits its applicability in practical engineering simulations. To address this challenge, we introduce a simplified kinetic model by approximating the non-local Enskog collision term using a first-order Taylor expansion in molecular diameter. The zeroth-order term is replaced by the Shakhov model to ensure the correct Prandtl number (Pr), and the first-order derivatives are evaluated by substituting the distribution function with a Maxwellian. Additionally, a second-order velocity term is retained to recover the correct bulk viscosity (Wang et al., 2020; Su et al., 2023). The resulting form of the collision term is given by

$$\Omega = J_S + J_e, \quad (7)$$

where the Shakhov model-like part  $J_S$  is

$$J_S = \frac{f^{eq} - f}{\tau} + \frac{f^{eq}}{\tau} \frac{2m(1 - Pr)\mathbf{q}^K \cdot \mathbf{C}}{5n(k_B T)^2} \left( \frac{mC^2}{2k_B T} - \frac{5}{2} \right), \quad (8)$$

and the excess part  $J_e$  is

$$J_e = -\rho b \chi f^{eq} \left\{ \mathbf{C} \cdot \left[ \frac{2}{n} \frac{\partial n}{\partial \mathbf{x}} + \frac{1}{T} \frac{\partial T}{\partial \mathbf{x}} \left( \frac{3mC^2}{10k_B T} - \frac{1}{2} \right) \right] \right. \\ \left. + \frac{2m}{5k_B T} \mathbf{C} \mathbf{C} : \frac{\partial}{\partial \mathbf{x}} \mathbf{u} - \left( 1 - \frac{mC^2}{5k_B T} \right) \left( \frac{\partial}{\partial \mathbf{x}} \cdot \mathbf{u} \right) \right\} \\ - \rho b \mathbf{C} f^{eq} \cdot \frac{\partial \chi}{\partial \mathbf{x}} \\ + \frac{\partial}{\partial \mathbf{x}} \cdot \left[ f^{eq} \frac{\varpi}{nk_B T} \left( \frac{\partial}{\partial \mathbf{x}} \cdot \mathbf{u} \right) \mathbf{C} \left( \frac{mC^2}{2k_B T} - \frac{3}{2} \right) \right]. \quad (9)$$

Here,  $\varpi$  denotes the bulk viscosity, and  $f^{eq}$  is the local Maxwellian distribution function, given by

$$f^{eq} = n \left( \frac{m}{2\pi k_B T} \right)^{3/2} \exp \left( -\frac{mC^2}{2k_B T} \right), \quad (10)$$

where  $n$  is the number density,  $T$  is the temperature,  $\mathbf{u}$  is the bulk velocity, and  $\mathbf{q}^K$  is the kinetic contribution to the heat flux. These macroscopic quantities are obtained from the velocity moments of the distribution function. The corresponding equation of state (EoS) derived from this model takes a generalized van der Waals form:

$$p = nk_B T (1 + \rho b \chi) - a n^2, \quad (11)$$

where  $b = 2\pi\sigma^3/3m$ ,  $\chi$  is the pair correlation function and  $a$  is the Vlasov parameter. Both  $\chi$  and  $a$  are treated as adjustable constants. This equation describes the complex dependence of pressure on number density and temperature, and serves as the basis for determining the critical parameters of the fluid. Specifically, the critical point is identified using the standard conditions:

$$\left( \frac{\partial p}{\partial n} \right)_{T=T_c, n=n_c} = 0, \quad \left( \frac{\partial^2 p}{\partial n^2} \right)_{T=T_c, n=n_c} = 0. \quad (12)$$

**Table 1**

The Vlasov term, critical and triple point parameters of Argon. All values are normalized by Avogadro constant  $N_A$

$aN_A^2(Jl/mol^2)$	$n_c/N_A(mol/l)$	$T_c(K)$	$n_{tr}/N_A(mol/l)$	$T_{tr}(K)$
162.5	13.41	150.69	35.47	83.81

To accurately reproduce the thermodynamic properties of Lennard-Jones fluids, we modify the EV-form equation of state by introducing a generalized approach for determining the pair correlation function  $\chi$  and the Vlasov parameter  $a$ . This method ensures consistency with key reference data such as the critical and triple points. As proposed in Benilov and Benilov (2018, 2019), the Vlasov parameter  $a$  is determined by fitting a linear relation to empirical data on the non-ideal component of the per-molecule internal energy of Lennard-Jones fluids. Meanwhile, the pair correlation function  $\chi$  is derived from an empirical function  $\Phi$ , which characterizes the non-ideal contribution to the fluid's entropy, and is introduced as:

$$\Phi = \rho b + a_1(\rho b)^2 + a_2(\rho b)^3 + a_3(\rho b)^4 + a_4(\rho b)^5, \quad (13)$$

satisfying

$$\chi = \frac{d\Phi}{d(\rho b)}. \quad (14)$$

This formulation provides sufficient flexibility to fit multiple thermodynamic constraints simultaneously. To ensure consistency with the critical point, the parameters  $a_{1,2,3,4}$  are calibrated using the Eq. 12. For the triple point, the per-molecule Gibbs free energy  $G$  is introduced:

$$G = k_B T [\ln(nT^{-3/2}) + \Phi + \frac{3}{2\pi} \rho b \Phi'] - 2an, \quad (15)$$

which is equivalent to the chemical potential for a single-component fluid. According to Benilov and Benilov (2019), the coexistence conditions at the triple point require

$$p(n_v, T_{tr}) = p(n_l, T_{tr}), \quad G(n_v, T_{tr}) = G(n_l, T_{tr}), \quad (16)$$

where the liquid-phase number density at the triple point is given by

$$n_{ltr} \sigma^3 = 1. \quad (17)$$

By simultaneously solving Eqs. 12, 16, and 17, the empirical coefficients in Eq. 14 can be uniquely determined.

This methodology provides a general framework that can be applied to all Lennard-Jones fluids. As an example, we apply it to Argon. The relevant thermodynamic parameters and the fitted value of the Vlasov term are listed in Table 1.

The fitted values for the empirical coefficients in Eq. 14 are:

$$\begin{aligned} a_1 &= -0.4133, & a_2 &= 1.0506, \\ a_3 &= -0.6693, & a_4 &= 0.1556. \end{aligned} \quad (18)$$

Substituting these values into Eq. 11 yields a calibrated equation of state that accurately captures both the critical and triple-point thermodynamic behavior of Argon.

Finally, the relaxation time  $\tau = \mu/nk_B T$ , while the shear viscosity of dense gas can be obtained by

$$\mu = \frac{\mu^*}{\chi} \left(1 + \frac{2}{5}\rho b\chi\right)^2 + \frac{3}{5}\varpi, \quad (19)$$

where  $\mu^*$  is the shear viscosity at the reference temperature, and the bulk viscosity is  $\varpi = \mu^* \chi (\rho b)^2$ . The thermal conductivity  $\kappa$  for dense gas can be calculated through

$$\kappa = \frac{\kappa^*}{\chi} \left(1 + \frac{3}{5}\rho b\chi\right)^2 + c_v \varpi, \quad (20)$$

where  $\kappa$  is the thermal conductivity at the reference pressure,  $c_v = 3k_B/2m$  is the specific heat capacity at constant volume. Finally, the  $Pr$  can be obtained through

$$Pr = \frac{2}{3} \frac{(1 + \frac{2}{5}\rho b\chi)^2 + \frac{3}{5}(\rho b\chi)^2}{(1 + \frac{3}{5}\rho b\chi)^2 + \frac{2}{5}(\rho b\chi)^2}. \quad (21)$$

### 3. Results and Discussion

The kinetic model is first validated by examining the equilibrium properties of a liquid–vapour system. To obtain the liquid–vapour coexistence curve, a liquid slab is initialized at the center of the simulation domain, surrounded by its vapour phase. The length of computation domain is set as  $L$ . Periodic boundary conditions are applied in both directions, and the temperature is maintained uniformly throughout the entire domain, as shown in Figure 1.

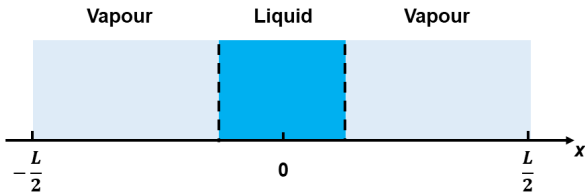


Figure 1: Schematic of the simulation setup

The simulation results are compared with those obtained from the original EV equation as well as the experimental data for Argon, as shown in Figure 2(a). As seen in the figure, for the results obtained from the original EV equations, the number density of the liquid phase exhibits significant deviation from the experimental values especially for low temperatures. This discrepancy primarily originates from the overly simplistic repulsive term in the Sutherland potential used in the original formulation. After applying modifications to EoS, i.e., introducing a more accurate expression of the thermodynamic properties of Lennard-Jones fluids, excellent agreement with the experimental data has been

achieved across a broad range of temperatures. In addition to the liquid–vapour coexistence curve, we also examine the equilibrium vapour pressure, which is calculated from the model via Eq. 11. As illustrated in Figure 2(b), the predicted vapour pressure is in good agreement with the experimental values over a broad range of temperatures, again confirming the validity of the kinetic model under equilibrium conditions. To further broaden the applicability of the model, we extend the simulation to two dimension and place a single droplet within the computational domain. In this setup, we focus on verifying the equilibrium properties of the droplet and evaluate the surface tension coefficient  $\gamma$  using the Young-Laplace equation

$$p_l - p_v = \frac{\gamma}{R}, \quad (22)$$

where  $p_l$  and  $p_v$  are the pressures in the liquid and vapour phases, respectively, and  $R$  is the radius of the droplet. The computed surface tension coefficient is then compared with the experimental data, as shown in Figure 2(c). The close agreement between the simulation and experimental data in all three quantities, liquid–vapour coexistence curve, vapour pressure, and surface tension, demonstrates that the proposed kinetic model can accurately capture the equilibrium behaviour of Lennard-Jones fluids in liquid–vapour systems. Slight over-estimate of the surface tension coefficient may attribute to the high-order curvature effect, which has been neglected in Eq.22 (Lulli, Biferale, Falcucci, Sbragaglia and Shan, 2022).

After the model validation, we employ our kinetic model to simulate non-equilibrium evaporation process. The simulation setup is also given by Figure 1. The absorbing walls are set on the boundaries, where the particles can only go outward and no particles are allowed to enter. The macroscopic profiles, including the number density, temperature, and bulk velocity, are shown in Figure 3(a). In the figure, the distance is normalized by the molecular diameter, the number density is normalized by  $1/\sigma^3$ , temperature is normalized by the room temperature, and the bulk velocity is normalized by the most probable molecular velocity. The difference to the equilibrium simulations is that the temperature decreases from the center to the boundary, while the number density has a slight increase due to the cooling effect. Since the particles are leaving on the boundaries, the velocity increases in the interface and vapour regions.

In addition to the variation of macroscopic parameters, particular attention is given to the molecular velocity distribution function, as its characteristics can help explain why the classical HK relation becomes inaccurate under strong evaporation conditions. We select several positions for analysis: near the end of the liquid phase ( $x = 11$ ), within the interface region ( $x = 13$ ), at the early stage of the vapour phase ( $x = 14.5$  and  $x = 15$ ), and closer to the boundary in the vapour phase ( $x = 17$ ). All the positions are also indicated by black hollow stars, from left to right, on the number density profile in Figure 3(a). For better comparison, the distribution function  $f$  is normalized by its maximum value at each position, and the molecular



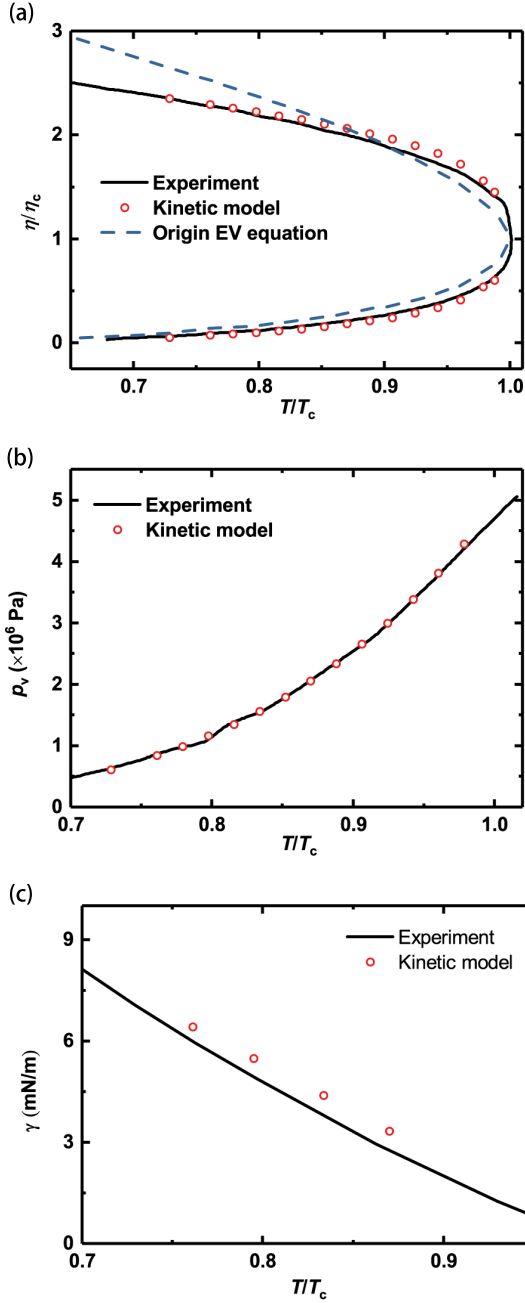


**Figure 2:** Comparison between the results obtained from kinetic model and experiment under different temperatures: (a) reduced number density; (b) vapour pressure; (c) surface tension coefficient. For better illustration, the liquid–vapour coexistence curve obtained from the original EV equation is shown in the figure (a)

velocity  $\xi$  is normalized by the molecular most probable velocity. As shown in Figure 3(b), the velocity distribution function closely follows the Maxwellian distribution in the high density regions, including the liquid phase and interface region. However, as the position approaches the vapour region, deviations emerge in the negative velocity range due

to insufficient molecular collisions in these low density regions, while the positive velocity region still roughly follows the Maxwellian. Notably, the bulk velocity becomes increasingly pronounced as the position approaches the boundary, due to the continuous outflow of particles into the vacuum. The onset of deviation is clearly visible, providing evidence for the breakdown of the HK relation, which is caused by two key factors: first, the velocity distribution function deviates from the Maxwellian in the vapor region adjacent to the liquid–vapour interface; second, the influence of bulk motion becomes increasingly significant near the vapour side, leading to a noticeable shift of the distribution, as illustrated by the case at  $x = 17$ . Not only can these findings provide in-depth understanding of the flow characteristics of liquid–vapour systems under strong evaporation, but also lay a solid foundation for an improved HK relation for strong non-equilibrium evaporation.

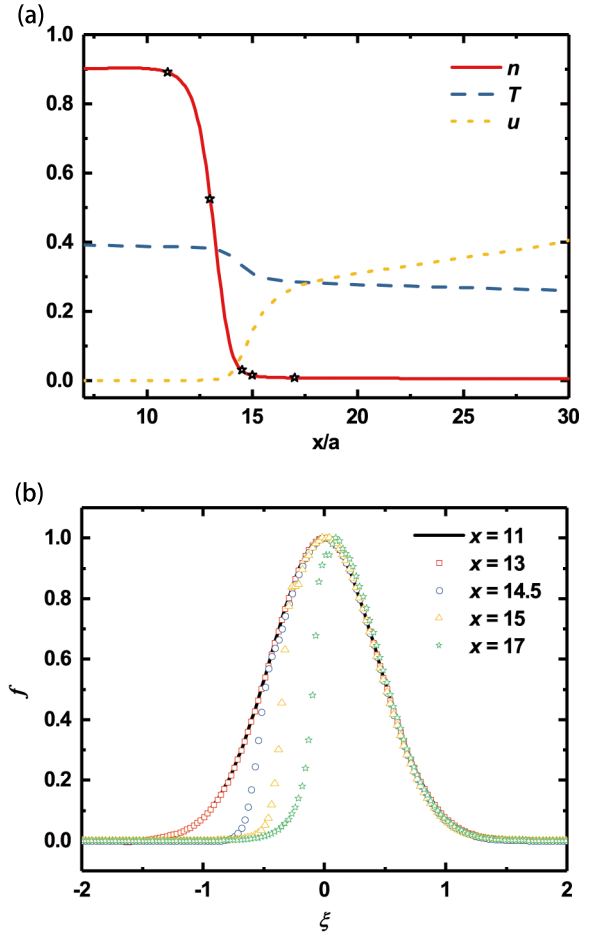


**Figure 3:** (a) Profiles of number density, temperature, and bulk velocity during evaporation into vacuum; (b) Velocity distribution functions at different positions:  $x = 11, 13, 14.5, 15$  and  $17$ . These positions are also denoted by black hollow stars in the figure (a).

## 4. Conclusions

In this letter, we developed a kinetic model capable of accurately reproducing the fluid properties of Lennard-Jones fluids. Starting from the Enskog equation, we simplified the collision term using a Taylor expansion and modelled molecular interactions with the Sutherland potential. To capture the thermodynamic behavior of real fluids, we calibrated the equation of state by matching key parameters, namely, the critical temperature and density, and the triple-point temperature and density. The model was validated against the experimental and molecular simulation data for Argon, showing good agreement in predicting the liquid–vapour coexistence curve, equilibrium vapour pressure, and surface tension coefficient. These results confirm the model is able to reproduce the essential thermodynamic properties of Lennard-Jones fluids. Furthermore, we applied the model to a non-equilibrium evaporative flow and analyzed the velocity distribution function at various spatial positions. The results reveal a clear deviation from the Maxwellian distribution in the negative velocity region of the beginning of vapour phase, highlighting inappropriateness of the equilibrium assumption underpinning the classical Hertz–Knudsen relation. The proposed approach can also be used to modify the Enskog–Vlasov model for other real fluids.

## References

- Barbante, P.F., Frezzotti, A., Gibelli, L., 2015. A kinetic theory description of liquid menisci at the microscale. *Kinet. Relat. Models* 8, 235–254.
- Benilov, E.S., Benilov, M.S., 2018. Energy conservation and H theorem for the Enskog–Vlasov equation. *Phys. Rev. E* 97, 062115.
- Benilov, E.S., Benilov, M.S., 2019. Peculiar property of noble gases and its explanation through the Enskog–Vlasov model. *Phys. Rev. E* 99, 012144.
- Busuioc, S., Gibelli, L., 2020. Mean-field kinetic theory approach to langmuir evaporation of polyatomic liquids. *Phys. Fluids* 32.
- Chen, F., Gang, T., Chen, L., 2024. Evaporation mechanisms during droplet levitation and coalescence based on molecular dynamics. *Theor. Appl. Mech. Lett.* 14, 100533.
- Chung, T.H., Ajlan, M., Lee, L.L., Starling, K.E., 1988. Generalized multiparameter correlation for nonpolar and polar fluid transport properties. *Ind. Eng. Chem. Res.* 27, 671–679.
- Dong, Y., Poredoš, P., Ma, Q., Wang, R., 2022. High-yielding and stable desalination via photothermal membrane distillation with free-flow evaporation channel. *Desalination* 543, 116103.
- Enskog, D., 1922. *Kinetische Theorie der Wärmeleitung: Reibung und Selbst-diffusion in gewissen verdichteten gasen und flüssigkeiten*. Almqvist & Wiksells boktryckeri-a.-b.
- Frezzotti, A., Barbante, P., 2017. Kinetic theory aspects of non-equilibrium liquid-vapor flows. *Mech. Eng. Rev.* 4, 16–00540.
- Frezzotti, A., Gibelli, L., Lorenzani, S., 2005. Mean field kinetic theory description of evaporation of a fluid into vacuum. *Phys. Fluids* 17.
- Graur, I.A., Gatapova, E.Y., Wolf, M., Batueva, M.A., 2021. Non-equilibrium evaporation: 1D benchmark problem for single gas. *Int. J. Heat Mass Transfer* 181, 121997.
- Grmela, M., 1971. Kinetic equation approach to phase transitions. *J. Stat. Phys.* 3, 347–364.
- Hertz, H., 1882. Ueber die verdunstung der flüssigkeiten, insbesondere des quecksilbers, im luftleeren raume. *Ann. Phys* 253, 177–193.
- Homes, S., Frezzotti, A., Nitzke, I., Struchtrup, H., Vrabec, J., 2025. Heat and mass transfer across the vapor-liquid interface: A comparison of molecular dynamics and the Enskog–Vlasov kinetic model. *Int. J. Heat Mass Transfer* 242, 126828.
- John, B., Enright, R., Sprittles, J.E., Gibelli, L., Emerson, D.R., Lockerby, D.A., 2019. Numerical investigation of nanoporous evaporation using direct simulation Monte Carlo. *Phys. Rev. Fluids* 4, 113401.
- John, B., Gibelli, L., Enright, R., Sprittles, J.E., Lockerby, D.A., Emerson, D.R., 2021. Evaporation from arbitrary nanoporous membrane configurations: An effective evaporation coefficient approach. *Phys. Fluids* 33.
- Karkheck, J., Stell, G., 1981. Kinetic mean-field theories. *J. Chem. Phys.* 75, 1475–1487.
- Knudsen, M., 1915. Die maximale verdampfungsgeschwindigkeit des quecksilbers. *Ann. Phys* 352, 697–708.
- Labuntsov, D.A., Kryukov, A.P., 1979. Analysis of intensive evaporation and condensation. *Int. J. Heat Mass Transfer* 22, 989–1002.
- Li, R., Wang, J., Xia, G., 2021. Theoretical and numerical study of nanoporous evaporation with receded liquid surface: effect of Knudsen number. *J. Fluid Mech.* 928, A9.
- Li, R., Yan, Z., Xia, G., 2023. Effect of inter-pore interference on liquid evaporation rates from nanopores by direct simulation Monte Carlo. *Phys. Fluids* 35.
- Li, S., Su, W., Shan, B., Li, Z., Gibelli, L., Zhang, Y., 2024. Molecular kinetic modelling of non-equilibrium evaporative flows. *J. Fluid Mech.* 994, A16.
- Lulli, M., Biferale, L., Falcucci, G., Sbragaglia, M., Shan, X., 2022. Mesoscale perspective on the Tolman length. *Phys. Rev. E* 105, 015301.
- Meland, R., Ytrehus, T., 2003. Evaporation and condensation Knudsen layers for nonunity condensation coefficient. *Phys. Fluids* 15, 1348–1350.
- Persad, A.H., Ward, C.A., 2016. Expressions for the evaporation and condensation coefficients in the Hertz–Knudsen relation. *Chemical reviews* 116, 7727–7767.
- Shan, B., Su, W., Gibelli, L., Zhang, Y., 2023. Molecular kinetic modelling of non-equilibrium transport of confined van der Waals fluids. *J. Fluid Mech.* 976, A7.
- Shan, B., Torrilhon, M., Guo, Z., Zhang, Y., 2025. Molecular kinetic modelling of nanoscale confined flows. *J. Fluid Mech.* 1012, A20.
- Sobrinho, L., 1967. On the kinetic theory of a van der Waals gas. *Can. J. Phys.* 45, 363–385.
- Su, W., Gibelli, L., Li, J., Borg, M.K., Zhang, Y., 2023. Kinetic modeling of nonequilibrium flow of hard-sphere dense gases. *Phys. Rev. Fluids* 8, 013401.
- Vaartstra, G., Zhang, L., Lu, Z., Díaz-Marín, C.D., Grossman, J.C., Wang, E.N., 2020. Capillary-fed, thin film evaporation devices. *J. Appl. Phys.* 128.
- Wang, J., Wang, Y., Li, B., Wang, Q., Meng, S., Chen, R., Wu, H., Wang, F., 2025. Molecular understanding of phase behavior of hydrocarbon mixtures in nanopores and their influence on recovery dynamics. *Theor. Appl. Mech. Lett.* 15, 100589.
- Wang, P., Wu, L., Ho, M.T., Li, J., Li, Z., Zhang, Y., 2020. The kinetic Shakhov–Enskog model for non-equilibrium flow of dense gases. *J. Fluid Mech.* 883, A48.